Received: 2 March 2023 | Revised: 25 September 2023 | Accepted: 29 September 2023

DOI: 10.1002/fuce.202300035

Fuel Cells
From Fundamentals to Systems

RESEARCH ARTICLE

Impedance analysis of electrolyte processes in a solid oxide cell

Felix Kullmann[1] | **Cedric Grosselindemann**[1] | **Luis Salamon**[1] | **Franz-Martin Fuchs**[2] | **André Weber**[1]

[1]Karlsruhe Institute of Technology (KIT), Institute for Applied Materials – Electrochemical Technologies (IAM-ET), Karlsruhe, Germany

[2]Kerafol Keramische Folien GmbH & Co. KG, Eschenbach, Germany

Correspondence
Felix Kullmann, Karlsruhe Institute of Technology (KIT), Institute for Applied Materials – Electrochemical Technologies (IAM-ET), Adenauerring 20b, 76131 Karlsruhe, Germany.
Email: felix.kullmann@kit.edu

Funding information
Bundesministerium für Bildung und Forschung, Grant/Award Numbers: BMBF 03HY124C, BMBF 03SF0622E

Abstract

Electrochemical impedance spectroscopy and the distribution of relaxation times are powerful tools to study polarization processes in solid oxide cells (SOC). Commonly the measured polarization resistance is solely attributed to polarization phenomena in the electrodes whereas the electrolyte is assumed to act as purely ohmic series resistance.

In this study an electrolyte supported SOC is investigated by impedance spectroscopy from the nominal operating temperature range of 700–900°C down to temperatures as low as 350°C. At such low temperatures the dielectric polarization of the electrolyte is shifted into the accessible frequency range, providing access to additional processes which are deconvoluted and quantified. It is discussed to which extent the additional layers like gadolinia doped ceria diffusion barrier and electrode layers influence the electrolyte processes as grain and grain boundary.

KEYWORDS
distribution of relaxation times, electrochemical impedance spectroscopy, electrolyte processes, electrolyte supported cell, low temperature, SOC

1 | INTRODUCTION

The commercialization of solid oxide cells (SOCs) requires a high cell performance and thus low area-specific resistance (ASR) values of the individual layers and their interfaces in the cell. The application of advanced materials, offering excellent intrinsic properties, is often limited by an insufficient compatibility towards other cell components. Interactions at interfaces taking place during processing and/or cell operation, as interdiffusion or secondary phase formation, often restrict the cell performance.

Well known examples are insulating zirconate interlayers formed between (La,Sr)(Co,Fe)O_3 (LSCF) air electrodes and zirconia-based electrolytes [1–5] or the interdiffusion of Ni from the fuel electrode into zirconia electrolytes [6–10]. To avoid them, interdiffusion barrier layers are implemented [1, 2, 5, 11] resulting in complex multilayered electrolytes.

In case of LSCF air electrodes a barrier layer of doped ceria (commonly CGO—gadolinia doped ceria) is placed between LSCF and YSZ to prevent zirconate formation [1, 2, 5, 11]. In the Ni/CGO anode a barrier layer of CGO also improves the cell performance [12]. On the other hand, interdiffusion between CGO and YSZ [2, 13–16] during sintering results in an interdiffusion layer with up to one order of magnitude lower conductivity [14]. Thus, morphology and sintering conditions of the ceria layer have to be optimized to prevent zirconate formation but simultaneously

avoid severe interdiffusion. At the fuel electrode, the interdiffusion of NiO into an 8YSZ-electrolyte during sintering [7, 8] and the subsequent reduction of NiO to metallic Ni during operation leads to an irreversible decrease in electrolyte conductivity [6, 8]. The reason for this conductivity loss is a phase transformation from cubic to tetragonal [6, 8–10]. The phase of YSZ is strongly dependent on the yttrium amount in the zirconia oxide. A high amount of 10 mol.% Y_2O_3 in zirconium oxide stabilize the YSZ. Doped with Ni, it shows almost no changes in conductivity during operation in reducing atmosphere [17] compared to 8YSZ. Over the years the intensive research lead to an enhanced understanding of material interactions and the subsequent impact on the cell performance. But due to high sintering temperatures, which are necessary to connect the different layers mechanically, material interactions are still challenges in the SOC and are sometimes unavoidable [2]. Furthermore, minor changes in the fabrication process like a different supplier of the powder could lead to huge differences in material interactions and subsequently in cell performance [18].

To optimize SOCs, a thorough understanding of the different ASR-contributions is mandatory. This is not limited to electrochemical processes in electrodes, further processes related to the ionic transport in the cell as grain and grain boundary conductivities of pristine electrolytes, interdiffusion layers and secondary phases as well as the impact of electrodes on the electrolyte conductivity have to be considered as well. Especially in ESCs these contributions can be dominant.

Whereas electrochemical processes can be deconvoluted from operando impedance spectroscopy by the distribution of relaxation times (DRT) analysis [19, 20], the processes in the electrolyte layer are often inaccessible due to their high relaxation frequencies and thus are cumulated in the ohmic resistance of the cell. To deconvolute such electrolyte processes from impedance measurements, their relaxation frequencies f_0 have to be shifted into the accessible frequency range, which can be achieved by impedance measurements at temperatures significantly below the nominal operating temperature of the cell.

In this contribution electrolyte supported cells consisting of LSCF air electrode / CGO interlayer / 3YSZ electrolyte substrate / CGO interlayer / Ni/CGO fuel electrode are investigated. Comparable cells are intensively investigated at nominal operation temperature of the SOC [21, 22], where the electrode processes are accessible and the relaxation frequencies of the electrolyte processes are far above the measurable frequency range and thus attributed to the ohmic resistance of the cell. To analyze the impact of the two electrode materials on the grain and grain boundary process of the electrolyte separately, different types of symmetrical cells were applied and impedance spectroscopy was performed at temperatures between 350 and 850°C. Here, the dielectric polarization behavior of grain and grain boundaries in the electrolyte exhibits relaxation frequencies in the kHz range [23–27]. This enables a quantification of the related resistance values and provides information how air/fuel electrode and CGO interlayers affect the ohmic resistance contributions of the 3YSZ electrolyte.

2 | EXPERIMENTAL

The electrolyte supported cells, manufactured by Sunfire GmbH, exhibit an active area of 1 cm^2. The electrolyte consists of 3 mol.% Y_2O_3 doped zirconium oxide (3YSZ) provided by Kerafol GmbH & Co. KG. The full cell consists of LSCF air electrode / CGO interlayer / 3YSZ electrolyte / CGO interlayer / Ni/CGO fuel electrode. Next to full cells, symmetrical cells were investigated. In case of the symmetrical fuel electrode, both sides of the electrolyte are coated with a CGO-interlayer and a Ni/CGO fuel electrode by screen printing (Figure 1a). After drying, the layers were cofired. For symmetrical air electrode cells (Figure 1b), the

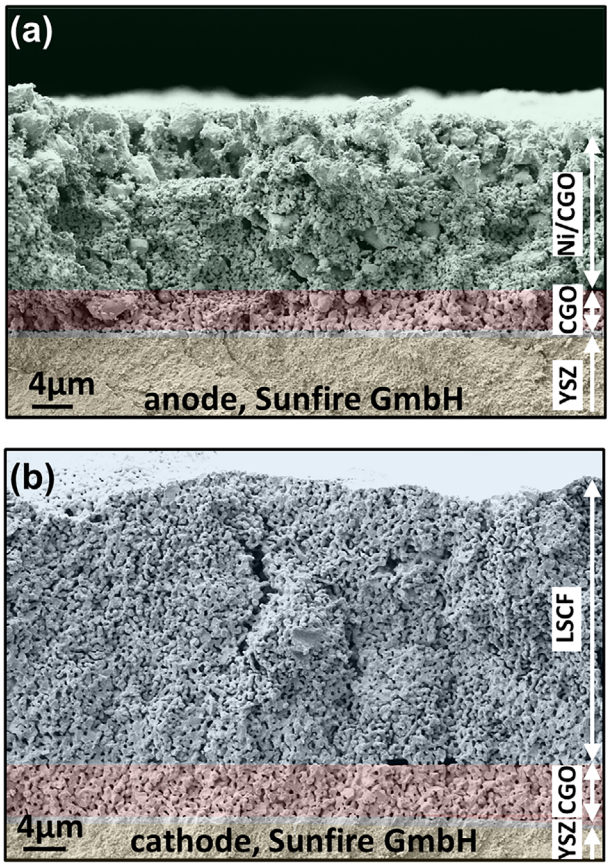

FIGURE 1 Scanning electron microscope (SEM) cross sections of (a) anode and (b) cathode layer.

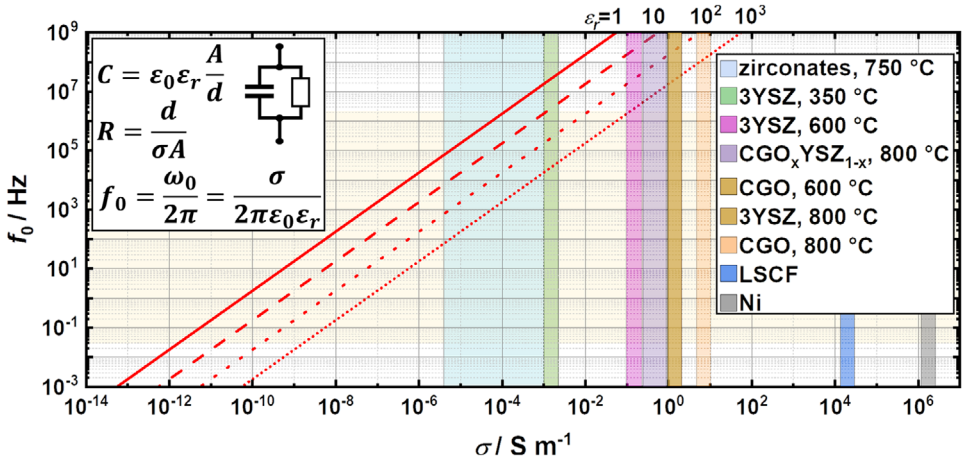

FIGURE 2 Link between the conductivity σ, characteristic frequency f_0 and the relative permittivity ε_r of materials like nickel [34], 3YSZ, CGO [33, 35, 36], (La,Sr)(Co,Fe)O_3 (LSCF) [37], and secondary phases like CGO_x-YSZ_{1-x} [14] and zirconates [4] at different temperatures. ε_0 describes the vacuum permittivity. The red lines consider different relative permittivities ε_r in between 1 and 1000, for the considered materials, values much below 100 have to be expected.

CGO/3YSZ/CGO multilayer electrolyte was produced similarly. Then the LSCF-layers were applied and sintered at a lower temperature. A third type of the symmetrical cells targeting the properties of the pristine electrolyte consist of a 3YSZ substrate with screen printed and sintered Pt-electrodes on both sides. The pristine electrolyte cell and the symmetrical anode cell are sintered with one sintering step whereas the symmetrical cathode and the full cell are sintered identically with two sintering steps. Thus, the anode in the full cell is exposed to a second sintering step at a lower temperature during the sintering process of the air electrode. It should be considered that the slightly different sintering procedures might have an influence on the grain and grain boundary resistance [26].

The test setup used in this study is described in [28]. For contacting anode and cathode, nickel and gold meshes respectively were applied, whereas the Pt-electrodes on the pristine electrolyte cell were contacted with platinum meshes. During the operation of the full cell, both electrodes were supplied by 250 sccm air and fuel gas, respectively. The symmetrical cells are located in an identical single chamber setup with a total gas flow rate of 500 sccm.

The electrochemical impedance spectroscopy measurements are performed by a Solartron 1260 in galvanostatic mode for the measurements above 600°C. The value of the sinusoidal stimulus is chosen that the voltage response of the electrode is ≤12 mV [28]. This approach was established at our institute over the last 20 years for measurements at high operation temperature and enables high quality impedance measurements in a frequency range between 30 mHz and 2 MHz. For the measurements in the lower temperature region below 600°C the potentiostatic mode is chosen since the cell resistance is much higher. Considering that the electrolyte processes are linear, a much higher amplitude of 200 mV can be applied leading to an operation of the Solartron in ranges of high resolution. For the symmetrical cell the voltage bias is set to zero. In case of the full cell the theoretical cell voltage is calculated and set as voltage bias. To guarantee valid impedance spectra the linear Kramers Kronig validity test was used [29]. For the impedance data analysis DRT and subsequent CNLS-fitting were applied to separate and quantify the loss processes in the spectrum.

3 | RESULTS AND DISCUSSION

At nominal operation temperature of the SOFC (700–900°C), the electrolyte losses are mainly ohmic, because the characteristic frequencies of the dielectric processes in the electrolyte layers are significantly above the frequency range of the impedance analyzer (30 mHz–2 MHz) applicable in high temperature test benches (Figure 2). Using equation 1

$$f_0 = \frac{\sigma}{2 \cdot \pi \cdot \varepsilon_0 \cdot \varepsilon_r}, \quad (1)$$

there is a direct link between characteristic frequency f_0, the relative permittivity ε_r/vacuum permittivity ε_0 and the conductivity σ of the respective material. If the conductivity decreases with lower temperatures the characteristic frequency also decreases and can shift into an accessible frequency range of the impedance analyzer. The lower conductivities of the secondary phases like zirconates [4] should have a much lower characteristic frequency in comparison to the pristine materials and might be visible

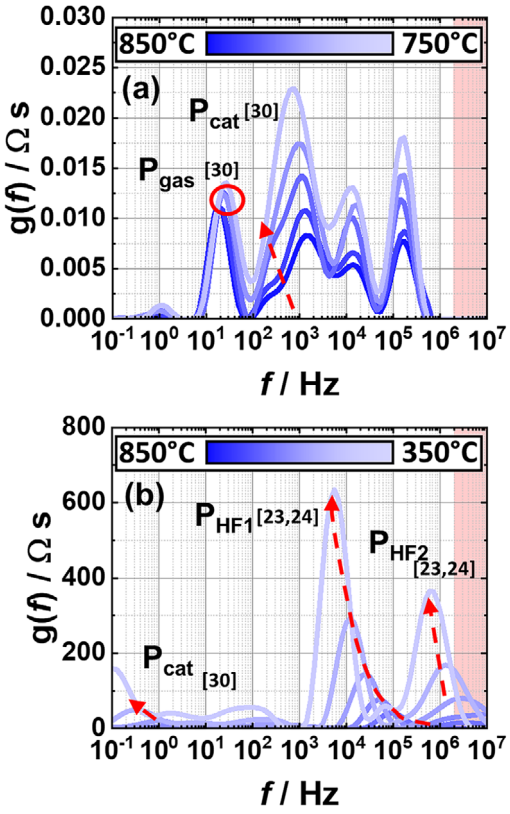

FIGURE 3 Distribution of relaxation times (DRT) of impedance spectra of a symmetrical cathode cell measured in the temperature range from 850°C to 750°C in (a) and down to 350°C in (b) in synthetic air. The red region is not measured, but extrapolated in the DRT calculation.

as a lower frequency peak in the spectrum according to Figure 2. CGO_xYSZ_{1-x} ($0.25 < x < 0.9$) and CGO instead could be overlapping with the 3YSZ electrolyte because of their similar conductivities at for instance 800°C. The conductivity of CGO_xYSZ_{1-x} is strongly dependent on the composition according to [14] and therefore also the characteristic frequency.

To investigate whether interdiffusion of NiO or elements of CGO and LSCF have an impact on the electrolyte processes different symmetrical cells were investigated by electrochemical impedance spectroscopy in a large temperature range as shown exemplary for the symmetrical cathode cell in Figure 3.

At nominal operation temperatures of the SOFC (850–750°C) mostly the electrode processes are visible and the relaxation frequencies of the electrolyte processes are far above the measurable frequency range and thus attributed to the ohmic resistance of the cell as shown in Figure 3a for a symmetrical cathode measured in synthetic air. It is clearly visible that the gas diffusion (P_{gas}) shows minor dependency on the temperature as to be expected [30]. At lower temperatures P_{gas} is covered by the thermally activated oxygen incorporation and oxygen ion diffusion in the LSCF-cathode (P_{cat}), which is often described by a Gerischer-element. At higher frequencies further thermally activated processes are visible which might be attributed to the charge transfer at the LSCF/CGO interface as well as the CGO/3YSZ interface including small amounts of secondary phases [2, 31]. In this operation conditions, the characteristic frequencies of the electrolyte processes are outside the frequency range of the impedance analyzer. To visualize the electrolyte processes in the impedance spectrum/DRT and to investigate them, a decrease in temperature is necessary. The characteristic frequencies of thermally activated processes will shift to lower frequencies, and the additional electrolyte processes become visible in the DRT.

Figure 3b pictures the DRT in a temperature range from 850°C down to 350°C. The first electrolyte process, which is called P_{HF1}, and the second high frequency process called P_{HF2} shift into the accessible frequency range. Due to the strong increase of the peak height, peak shifting is in this linear presentation of the y-axis hard to analyze. For a better visualization, the impedance evolutions over temperature are plotted with a logarithmic y-axis in Figure 4. It should be noted that the geometrical area underneath the peaks no longer corresponds to the related polarization resistance.

Figure 4a shows the DRTs of a symmetrical anode cell measured in 25/25/50 $H_2O/H_2/N_2$. The electrochemistry of the anode [21, 22] by the peaks LF_1 and LF_2 is strongly temperature dependent. The relaxation frequency of these peaks shifts to the lower end of the measured frequency range at lower temperatures. A gas diffusion process is not separable as it is overlapping with the electrode processes at high temperatures [21] and, as gas diffusion is not thermally activated, only comprises an insignificant contribution to the polarization resistance and DRT at lower operating temperatures. Simultaneously the high frequency electrolyte processes shift into the accessible frequency range and are fully visible at 350°C. According to [23, 25, 27, 32] the electrolyte process HF_1 at a lower relaxation frequency should represent the grain boundary resistance contribution and the second process HF_2 at a higher relaxation frequency the resistance contribution of the grains in the 3YSZ electrolyte substrate. This allocation is supported by the fact that HF_1 and HF_2 are occurring in all types of cells to a quite similar extent. Further peaks between LF_2 and HF_1, which are named MF_{1-3} in Figure 5c, are significantly smaller. They might be related to the interdiffusion zone between 3YSZ and CGO which should have a lower characteristic frequency according to Figure 2.

The DRTs of temperature variations of the pristine electrolyte cell measured in synthetic air and in $H_2/H_2O/N_2$ reveal some low frequency processes related to the Pt

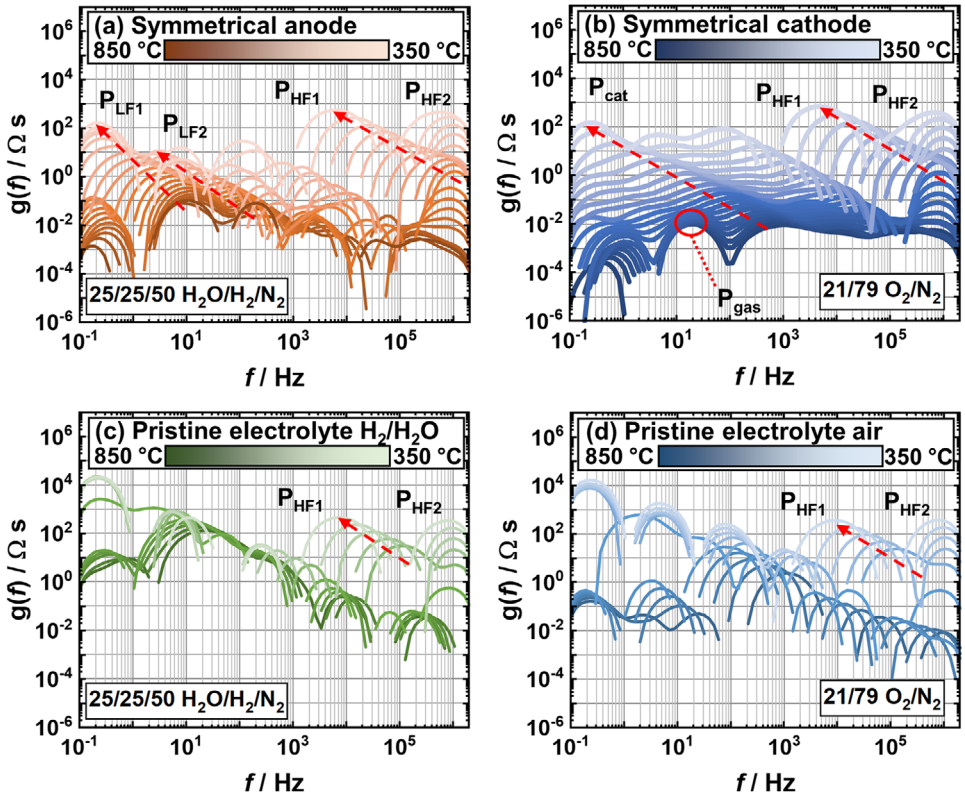

FIGURE 4 Distribution of relaxation times (DRT) of impedance spectra measured in the temperature range from 850°C down to 350°C of symmetrical anode cell (a), symmetrical cathode cell (b) and pristine electrolyte cell with Pt-electrodes in reducing (c) and oxidizing (d) atmospheres.

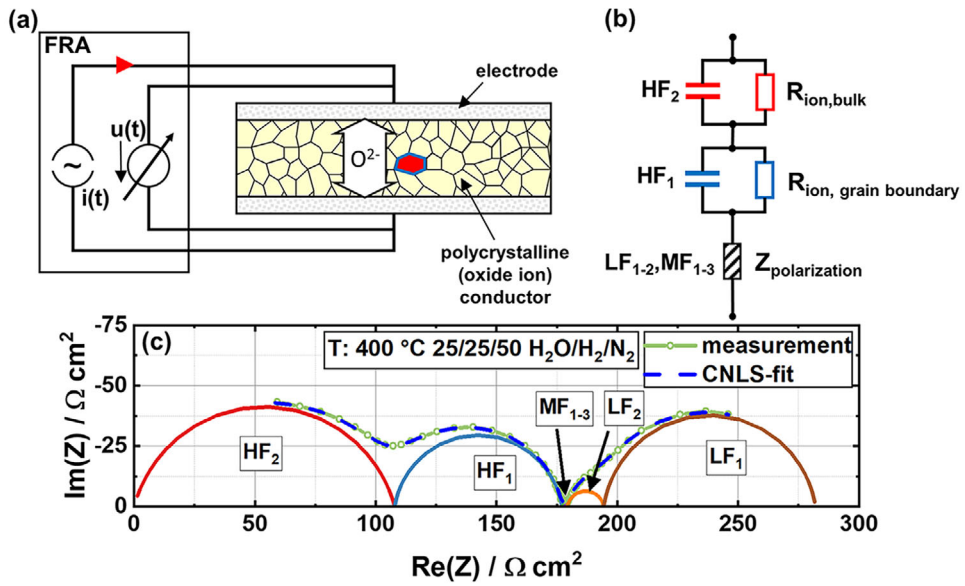

FIGURE 5 (a) Scheme of impedance measurement of polycrystalline conductors. (b) Equivalent circuit model consisting of RQ elements. (c) Impedance spectrum of a symmetrical anode cell measured at 400°C in 25/25/50 $H_2/H_2O/N_2$. The spectrum covers high and low frequency processes at least partly.

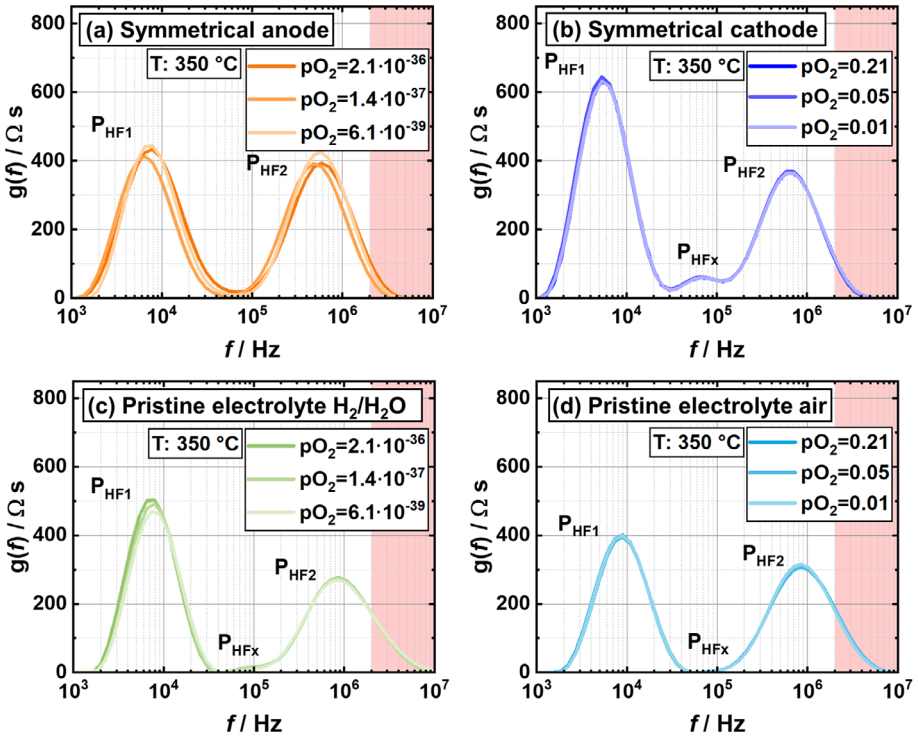

FIGURE 6 Gas mixture dependency of the symmetrical anode cell (a), cathode cell (b), and the pristine electrolyte cell in $H_2/H_2O/N_2$ (a and c) and in O_2/N_2 (b and d). The red region is not measured, but extrapolated in the distribution of relaxation times (DRT) calculation.

electrode, whose behavior differs in reducing and oxidizing atmosphere. Since the Pt-electrodes are only used for the electronic contact of the 3YSZ electrolyte/electrochemical reaction of oxygen and hydrogen respectively and should not have any influence to the electrolyte processes they are no part of further discussion. The impedance spectra also show two electrolyte processes HF_1 and HF_2, which are of interest in this study.

A scheme of the impedance spectroscopy in polycrystalline oxide ion conductors is pictured in Figure 5a. In the polycrystalline conductor, the oxygen ions are moving due to the sinusoidal stimulus and generate losses in grain (red, HF_2) and grain boundaries (blue, HF_1). These losses can be described by capacities in parallel to ohmic resistances or rather RQ elements as shown in Figure 5b. Figure 5c shows a typical impedance spectrum of a symmetrical anode cell at 400°C. At low frequencies, the anode process is partly covered, and at the higher frequencies, the electrolyte process HF_1 is fully and process HF_2 is partly covered in the spectrum. For better visualization the equivalent circuit elements used for fitting are plotted in the diagram. In the equivalent circuit model RQ elements are used to represent $LF_{1\text{-}2}$ [21], the $MF_{1\text{-}3}$ and the electrolyte processes $HF_{1\text{-}2}$. In Figure 5b the RQ elements for $LF_{1\text{-}2}$ and $MF_{1\text{-}3}$ are summarized as $Z_{polarization}$.

To study the question if the secondary phase formation or ceria interdiffusion into 3YSZ have an impact on the electrolyte processes at grain or grain boundary, in Figure 6 a variation of the gas mixtures is applied to the symmetrical cells at 350°C. Since electronic and ionic transport in ceria are expected to show a pO_2-dependency an impact to the electrolyte processes should be visible if there is an influence of ceria or an overlapping of the processes. In the diagrams, only the high frequency part representing the electrolyte processes is shown. For the symmetrical anode cell and the pristine electrolyte cell in Figure 6a,c a H_2/H_2O-variation was performed ranging from 25/25/50 to 2.5/47.5/50 $H_2O/H_2/N_2$. The DRTs of the symmetrical anode cell show no clear trend in HF_1 and HF_2, in case of the pristine electrolyte cell a minor impact on HF_1 is visible.

Possible explanations are that the interdiffusion zone is included in another peak with a lower characteristic frequency according to Figure 2 or the margin of the gas mixture is too small. Another explanation could be that since the whole electrolyte is about 80 µm thick, the impact of the interdiffused ceria or even the CGO barrier layer might be negligible. In case of thinner electrolyte layers such impact will be increased.

The DRT of the symmetrical cathode cell (b) and the pristine electrolyte cell (d) is measured during a O_2/N_2-variation from 21/79 to 1/99 O_2/N_2 ($pO_2 = 0.21 \ldots 0.01$). In this case no pO_2-dependency becomes visible. Since the ionic conductivity of CGO should be less influenced by the

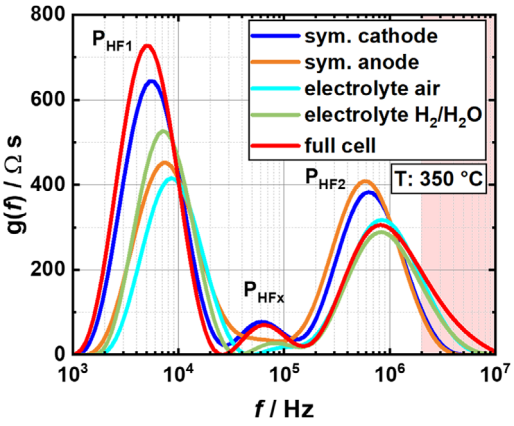

FIGURE 7 Comparison of distribution of relaxation times (DRTs) of the symmetrical cells and the full cell in different atmospheres. The anode is in each case exposed to 25/25/50 $H_2O/H_2/N_2$ and the cathode to synthetic air. The pristine electrolyte cell is measured in both atmospheres. The red region is not measured, but extrapolated in the DRT calculation.

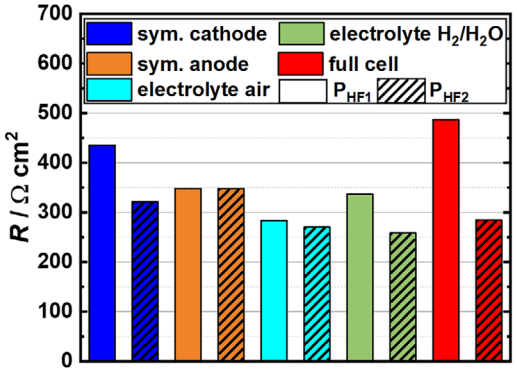

FIGURE 8 Fitting results of process HF_1 and HF_2 of the analyzed cells at 350°C in Ω cm^2.

oxygen partial pressure at high oxygen levels in oxidizing atmosphere [33], an impact is not to be expected.

In Figure 7, the electrolyte processes of the different investigated cells including symmetrical cells and full cell are compared at 350°C.

(i) Comparison of symmetrical anode cell and pristine electrolyte cell in $H_2/H_2O/N_2$ at 350°C:

The symmetrical anode cell and the pristine electrolyte cell are measured in 25/25/50 $H_2O/H_2/N_2$. Process HF_1, which should belong to the grain boundary, shows quite similar resistance (area underneath the peak) and relaxation frequency values for both cells (fit values are shown in Figure 8). Process HF_2, attributed to the bulk conductivity in the grains, shows a larger deviation. The pristine electrolyte cell exhibits a higher conductivity and relaxation frequency.

(ii) Comparison of symmetrical cathode cell and pristine electrolyte cell in air at 350°C:

The comparison between the symmetrical cathode cell and the pristine electrolyte cell both measured in synthetic air shows a significantly higher resistance and lower relaxation frequency for HF1 and HF_2 for the symmetrical cathode cell. The reason for this could be due to the additional CGO layer and the interdiffusion of elements from the LSCF cathode and/or the CGO layer into YSZ. In the spectrum of the symmetrical cathode cell shown in Figure 7 is also an additional peak with a minor resistance in comparison to HF_1 and HF_2 visible, which is named HF_x. It is more distinctive in the spectrum of the symmetrical cathode cell than the pristine electrolyte cell.

(iii) Comparison of symmetrical anode and cathode cell at 350°C:

The symmetrical anode and cathode cells are measured in 25/25/50 $H_2O/H_2/N_2$ and synthetic air, respectively. It can be seen that HF_1 shows a significant difference whereas HF_2 is approximately similar for both cells. The higher value of process HF_1 in the symmetrical cathode cell might be explained by the lower electrical conductivity of ceria in oxidizing atmosphere [33] or the diffusion of Co and Fe along the YSZ grain boundaries. The interdiffusion could be additionally affected by the different sintering procedure of the symmetrical cathode and anode cell. The additional peak HF_x is more distinctive in the symmetrical cathode cell spectrum than in the spectrum of the symmetrical anode cell.

(iv) Comparison between the pristine electrolyte cell in different atmospheres at 350°C:

HF_1 and HF_2 show differences between the pristine electrolyte cell measured in air and in $H_2/H_2O/N_2$. Factorial differences can be excluded, because both spectra were measured with the same cell. First the measurements took place in air, then in $H_2/H_2O/N_2$.

(v) Comparison between the full cell and the symmetrical cells at 350°C:

The comparison between the full cell tested in synthetic air / 25/25/50 $H_2O/H_2/N_2$ and the pristine electrolyte cells at 350°C shows a comparable value for HF_2 (Figures 7 and 8). The value of the symmetrical anode and cathode cell is higher. Process HF_1 shows the highest value for the full cell. By summing up half of the resistance from the symmetrical cathode and anode cell respectively and comparing it to the full cell we see differences. The differences could be induced by different sintering procedures [26], small differences in electrolyte thickness (between 82 µm and 86 µm) and minor temperature differences (<±2°C). The difference might also imply that the

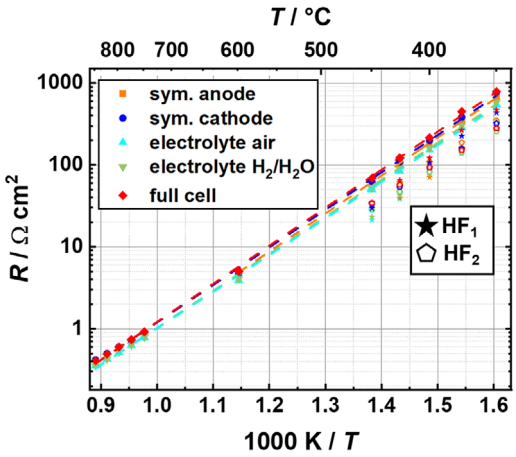

FIGURE 9 Resistance contribution of single electrolyte processes and the sum of the electrolyte processes of the analyzed cells in a temperature range from 350°C to 850°C. The anode is in each case exposed to 25/25/50 $H_2O/H_2/N_2$ and the cathode to synthetic air. The pristine electrolyte cell is measured in both atmospheres.

second sintering step of the anode in the full cell increase the loss process HF_1. Process HF_x shows a comparable peak height in the full cell and the symmetrical cathode cell. This might imply that this process is originated in the cathode.

Figure 9 compares the resistance contributions of the electrolyte layers of the different samples in a temperature range from 350°C to 850°C. At the lower temperatures (450–350°C), the resistance is calculated by the sum of the high frequency processes. At higher temperatures the ohmic resistance is chosen. It should be noted that a good agreement with relative errors <1% is achieved for a single activation energy per cell. The resistances of symmetrical cathode and anode cell are larger than the resistance of the pristine electrolyte cell, whereas the resistance of the full cell shows the highest values at temperatures below 600°C. The activation energies of the sum of the electrolyte processes of full cell (0.92 eV), symmetrical cathode cell (0.91 eV) and symmetrical anode cell (0.92 eV) are slightly higher than of the pristine electrolyte cell (air: 0.89 eV, $H_2O/H_2/N_2$: 0.90 eV). The measured values are similar to the reported values for pristine 3YSZ [24, 27] (0.95–1.0 eV).

Additionally, the single electrolyte processes HF_1 and HF_2 are plotted between 450 and 350°C. Process HF_1 is except for the symmetrical anode cell larger than HF_2 in lower temperatures (350°C), but smaller or equal at higher temperatures (450°C). In case of the symmetrical anode they are equal at 350°C and deviate from each other to higher temperatures while HF_1 is smaller than HF_2. The difference is explainable by the different activation energies of HF_1, which are in the range of 1–1.1 eV, and HF_2, which are in the range of 0.84 and 0.88 eV. The single activation energies of the cells are shown in Table 1. In literature [24] for the process HF_1 of 3YSZ (grain boundary) 1.15 eV is shown, for HF_2 (grain) 0.78 eV, which confirms a correct process assignment.

TABLE 1 Activation energies of the single electrolyte processes (HF_1 and HF_2) and of the total electrolyte resistance.

	HF_1	HF_2	HF_1+HF_2
$H_2O/H_2/N_2$		25/25/50	
Sym. anode cell	1.10 eV	0.86 eV	0.92 eV
Pristine electrolyte cell	1.04 eV	0.85 eV	0.90 eV
O_2/N_2		21/79	
Sym. cathode cell	1.05 eV	0.87 eV	0.91 eV
Pristine electrolyte cell	1.01 eV	0.88 eV	0.89 eV
O_2/N_2 / $H_2O/H_2/N_2$		21/79 / 25/25/50	
full cell	1.03 eV	0.84 eV	0.92 eV

The low temperature investigations of the two electrolyte processes showed the potential of the electrochemical impedance spectroscopy to investigate the impact of both electrodes sintered on the 3YSZ substrate in a rather simple and quick approach comparing to an expensive and time-consuming microstructural analysis. A comparison of the electrolyte resistances of the pristine and symmetrical cells could show an impact of the electrodes as expected. Explanations for the difference between the sum of half of the electrolyte resistances of anode and cathode cell and the full cell might be a slightly different sintering procedure and small differences in electrolyte thickness and operation temperature.

4 | CONCLUSION

In this study the high frequency processes of a symmetrical anode, a symmetrical cathode, a pristine electrolyte cell and the corresponding full cell were investigated by electrochemical impedance spectroscopy over a wide temperature and pO_2 range. Different measurement series in reducing and oxidizing atmospheres were performed.

At operating temperatures between 350°C and 450°C the DRT unfolded two main processes HF_1 and HF_2 attributed to grain boundary and grain resistances respectively. Oxygen partial pressure variations in oxidizing and reducing atmospheres at 350°C showed no significant impact on these processes. Comparing oxidizing and reducing conditions, differences were revealed even for the pristine electrolyte cells.

Higher values for HF_1 and HF_2 were observed for the full cell, symmetrical cathode and anode cell in comparison to the pristine electrolyte cell. This increase might be

attributed to the CGO barrier layer or interactions with the CGO layer and further interdiffusion of Ni and elements from the LSCF cathode respectively. By summing up half of the resistance from the symmetrical cathode cell and anode cell and comparing it to the full cell, we see differences. The differences could be induced by different sintering procedures, small differences in electrolyte thickness and minor temperature differences.

To evaluate the interactions on grain and grain boundary properties, a detailed microstructural and chemical analysis will be mandatory.

This study shows the potential of the electrochemical impedance spectroscopy in order to investigate all electrical and electrochemical processes occurring in the solid oxide cell during operation from low frequency gas diffusion processes to high frequency grain processes in the electrolyte.

ACKNOWLEDGMENTS

The authors thank the Sunfire GmbH and the Kerafol GmbH & Co. KG for the generous supply of the cells. They gratefully acknowledge funding by the Bundesministerium für Bildung und Forschung (BMBF 03HY124C and BMBF 03SF0622E).

Open access funding enabled and organized by Projekt DEAL.

ORCID

Felix Kullmann https://orcid.org/0000-0002-6653-5601
Cedric Grosselindemann https://orcid.org/0000-0002-9965-843X
André Weber https://orcid.org/0000-0003-1744-3732

REFERENCES

1. A. Kromp, J. Nielsen, P. Blennow, T. Klemensø, A. Weber, *Fuel Cells* **2013**, *13*, 598.
2. J. Szász, F. Wankmüller, V. Wilde, H. Störmer, D. Gerthsen, N. H. Menzler, E. Ivers-Tiffée, *J. Electrochem. Soc.* **2018**, *165*, F898.
3. H. Yokokawa, N. Sakai, T. Kawada, M. Dokiya, *Solid State Ion.* **1990**, *40/41*, 398.
4. F. W. Poulsen, N. van der Puil, *Solid State Ion.* **1992**, *53–56*, 777.
5. A. Mai, V. A. C. Haanappel, F. Tietz, I. C. Vinke, D. Stöver, *Proc. Electrochemical Society*, (Eds. S. C. Singhal, M. Dokiya), Paris, France **2003**, 525.
6. S. Linderoth, N. Bonanos, K. V. Jensen, J. B. Bilde-Sørensen, *J. Am. Ceram. Soc.* **2001**, *84*, 2652.
7. A. Müller, A. Weber, H. J. Beie, A. Krügel, D. Gersthen, E. Ivers-Tiffée, *Proc. 3rd European Solid Oxide Fuel Cell Forum*, (Ed. P. Stevens), Nantes, France **1998**, 353.
8. A. Lefarth, B. Butz, H. Störmer, A. Utz, D. Gerthsen, *ECS Trans.* **2011**, *35*, 1581.
9. V. Sonn, E. Ivers-Tiffée, *Proc. 8th European Solid Oxide Fuel Cell Forum*, (Eds. R. Steinberger-Wilckens, U. Bossel), Lucerne, Switzerland **2008**, B1005.
10. T. Shimonosono, H. Kishimoto, M. E. Brito, K. Yamaji, T. Horita, H. Yokokawa, *Solid State Ion.* **2012**, *225*, 69.
11. J. Peña-Martínez, D. Marrero-López, C. Sánchez-Bautista, A. J. dos Santos-García, J. C. Ruiz-Morales, J. Canales-Vazquez, P. Núñez, *Bol. Soc. Esp. Ceram. Vidr.* **2010**, *49*, 15.
12. A. Weber, S. Dierickx, N. Russner, E. Ivers-Tiffée, *ECS Trans.* **2017**, *77*, 141.
13. A. Tsoga, A. Naoumidis, A. Gupta, D. Stöver, *Mater. Sci. Forum* **1999**, *308–311*, 794.
14. A. Tsoga, A. Naoumidis, D. Stöver, *Solid State Ion.* **2000**, *135*, 403.
15. X. D. Zhou, B. Scarfino, H. U. Anderson, *Solid State Ion.* **2004**, *175*, 19.
16. A. Tsoga, A. Gupta, A. Naoumidis, P. Nikolopoulos, *Acta Mater.* **2000**, *48*, 4709.
17. W. G. Coors, J. R. O'Brien, J. T. White, *Solid State Ion.* **2009**, *180*, 246.
18. S. Golani, A. Weber, F. Wankmüller, W. Herzhof, C. Dellen, N. H. Menzler, *Proc. 15th European SOFC & SOE Forum*, (Eds. J. Mougin, J. Laurencin), Lucerne, Switzerland **2022**, A0901.
19. A. Leonide, V. Sonn, A. Weber, E. Ivers-Tiffée, *J. Electrochem. Soc.* **2008**, *155*, B36.
20. H. Schichlein, A. C. Müller, M. Voigts, A. Krügel, E. Ivers-Tiffée, *J. Appl. Electrochem.* **2002**, *32*, 875.
21. C. Grosselindemann, N. Russner, S. Dierickx, F. Wankmüller, A. Weber, *J. Electrochem. Soc.* **2021**, *168*, 124506.
22. M. Riegraf, R. Costa, G. Schiller, K. A. Friedrich, S. Dierickx, A. Weber, *J. Electrochem. Soc.* **2019**, *166*, F865.
23. J. E. Bauerle, *J. Phys. Chem. Solids* **1969**, *30*, 2657.
24. S. P. S. Badwal, *J. Mater. Sci. Lett.* **1987**, *6*, 1419.
25. B. Butz, P. Kruse, H. Störmer, D. Gerthsen, A. Weber, E. Ivers-Tiffée, *Solid State Ion.* **2006**, *177*, 3275.
26. M. Han, X. Tang, H. Yin, S. Peng, *J. Power Sources* **2007**, *165*, 757.
27. J. Luo, D. P. Almond, R. Stevens, *J. Am. Ceram. Soc.* **2000**, *83*, 1703.
28. D. Klotz, A. Weber, E. Ivers-Tiffée, *Electrochim. Acta* **2017**, *227*, 110.
29. M. Schönleber, D. Klotz, E. Ivers-Tiffée, *Electrochim. Acta* **2014**, *131*, 20.
30. A. Leonide, B. Rüger, A. Weber, W. A. Meulenberg, E. Ivers-Tiffée, *J. Electrochem. Soc.* **2010**, *157*, B234.
31. J. T. Szász, *Ph.D. Thesis*, Karlsruhe Institute for Technology (KIT), Karlsruhe, Germany **2019**.
32. J. R. Macdonald, E. Barsoukov, *Impedance Spectroscopy Theory, Experiment, and Applications*, John Wiley & Sons, Inc., Hoboken, USA, **2005**.
33. S. Wang, T. Kobayashi, M. Dokiya, T. Hashimoto, *J. Electrochem. Soc.* **2000**, *147*, 3606.
34. R. W. Powell, R. P. Tye, M. J. Hickman, *Int. J. Heat Mass Transfer* **1965**, *8*, 679.
35. C. Xia, M. Liu, *Solid State Ion.* **2002**, *152*, 423.
36. B. C. H. Steele, *Solid State Ion.* **2000**, *129*, 95.
37. J. W. Stevenson, T. R. Armstrong, R. D. Carneim, L. R. Pederson, W. J. Weber, *J. Electrochem. Soc.* **1996**, *143*, 2722.

How to cite this article: F. Kullmann, C. Grosselindemann, L. Salamon, F.-M. Fuchs, A. Weber, *Fuel Cells* **2023**, 1.
https://doi.org/10.1002/fuce.202300035